ADVANCED MATERIALS INTERFACES
www.advmatinterfaces.de

Aminoclay-Graphene Oxide Composite for Thin-Film Composite Reverse Osmosis Membranes with Unprecedented Water Flux and Fouling Resistance

Md Rabiul Islam, Pratishtha Khurana, Pillalamarri Srikrishnarka, Ankit Nagar, Madhuri Jash, Shantha Kumar Jenifer, Mohd Azhardin Ganayee, Mathava Kumar, and Thalappil Pradeep**

Present work attempts to incorporate aminoclay-graphene oxide composites into thin-film composite (TFC)-reverse osmosis membranes to improve the desalination efficiency of brackish water. The composite is coated on a polysulfone substrate as a result of interfacial polymerization of m-phenylene diamine and trimesoyl chloride, at different time durations. The prepared membranes are analyzed for their water permeation and salt rejection efficiencies using brackish feed water. The results indicated that the membrane loaded with 0.015 wt% of the composite delivered maximum flux at 20 bar pressure for 2000 ppm feed. Moreover, the water flow rate increased by ≈3.27 times (from 15.62 ± 0.36 to 50.28 ± 1.69 $Lm^{-2} h^{-1}$), compared to the unmodified TFC membrane. An enhancement in the salt rejection from 97.03 ± 1.07 to 99.51 ± 0.10% is also observed for the same feed water at 20 bar as compared to the unmodified membrane. Furthermore, antifouling tests with model bio-foulant humic acid revealed better stability and antifouling performance of the prepared membranes than the unmodified membranes under identical operating conditions. The membrane, therefore, assures high performance and lifetime owing to its mechanical and chemical stability, and hence suggests energy-efficient desalination.

1. Introduction

Water is the world's most precious resource, essential for the functioning of all life forms. Desalination using reverse osmosis (RO) has emerged as a promising method to eradicate the drinking water crisis.[1–7] An RO membrane generally consists of a polyester non-woven fabric upon which a polysulfone layer is casted. These two layers are porous, highly permeable, and provide mechanical support to the topmost layer. The polysulfone side of the membrane is coated with a cross-linked aromatic polyamide thin film by interfacial polymerization between the organic molecules (e.g., trimesoyl chloride, TMC) and aqueous (e.g., m-phenylene diamine, MPD) phases.[8–11] The presence of the active layer of polyamide improves the salt rejection, and antifouling properties of the membrane.[11,12] Additives including camphor sulfonic acid (CSA), triethylamine (TEA), and sodium lauryl sulfate (SLS) are also frequently used to enhance the membrane preparation by aiding the absorption of MPD on the polysulphone support.[12]

Despite copious advantages of membrane filtration systems, such as easy operation and high flexibility in technologies, they present some limitations, including chlorine sensitivity, and susceptibility to fouling, which impedes their large-scale applications.[13–15] In some cases, deposition of extra-cellular polymeric substances (EPS), soluble microbial products (SMP), and microbial cells in the pores resulting in a drop in flux and salt rejection capacity. The amide groups in the polyamide skin layer are also vulnerable to chlorine attack, even at a low chlorine dosage in the feed water.[16]

The polyamide chains allegedly undergo ring chlorination in the presence of chlorine, which disrupts hydrogen bonding between the chains and degrades the polymer matrix.[17] The disruption leads to a dramatic decline in the permeation flux, membrane life, and selectivity, which increases the required pressure for operation. Modification of the thin-film composite (TFC) membranes by adding different hydrophilic nanomaterials like carbon, alumina, silica zeolites, 2D materials, and their derivatives is common in order to combat these problems and improve water permeation characteristics.[8,18–28] Recently, several nanocomposites-based RO membranes have been explored extensively, as synergy of components enhances the physicochemical properties and increases thermal and

M. R. Islam, P. Khurana, P. Srikrishnarka, A. Nagar, M. Jash, S. K. Jenifer, M. A. Ganayee, M. Kumar, T. Pradeep
DST Unit of Nanoscience (DST UNS), and Thematic Unit of Excellence (TUE)
Department of Chemistry
Indian Institute of Technology Madras
Chennai 600 036, India
E-mail: pradeep@iitm.ac.in
M. Kumar
Environmental and Water Resources Engineering Division
Department of Civil Engineering
Indian Institute of Technology Madras
Chennai 600 036, India
E-mail: madhav@iitm.ac.in
The ORCID identification number(s) for the author(s) of this article can be found under https://doi.org/10.1002/admi.202100533.

DOI: 10.1002/admi.202100533

chemical stability of the resulting materials.[29] Besides, they can be readily incorporated onto the membrane by mixing them in the aqueous or organic phase before the fabrication reaction of the polyamide layer, or they can be bonded chemically to the surface of TFC via bonding agents.[19]

Among the most common additives used for TFC-RO membranes are graphene oxide (GO) and its derivatives, owing to their higher permeability, improved selectivity, and better chlorine tolerance than polyamide. GO is highly hydrophilic due to the presence of various oxygen-containing functional groups on its surfaces and edges, allowing better dispersion in water and enhancing the compatibility with polysulfone substrate via different covalent and non-covalent interactions.[30] GO forms hydrogen bonds with primary and secondary amines, in addition to covalent bonds with terminal free carboxyl groups of TMC in the linear portion of the polyamide layer.[31,32]

In the present work, we have investigated the effect of incorporating aminoclay-graphene oxide (AC-GO) composite on water flux, salt removal efficiency, and the antifouling tendency of the RO membranes. Aminoclay (AC) is an aminopropyl-functionalized magnesium phyllosilicate ($R_8Si_8Mg_6O_{16}(OH)_4$, where R is $CH_2CH_2NH_2$). It consists of octahedrally coordinated MgO/OH chains and an aminopropyl-functionalized silicate network on both sides.[33] The protonation of amine moiety makes it highly dispersible in water, enabling it to interact electrostatically with anions like $HAsO_4^{2-}$, CrO_4^{2-}, Fe $(CN)_6^{3-}$, F^-, NO^{3-}, and PO_4^{3-}, thereby facilitating their removal.[34,35] AC is also known to possess anti-algicidal properties, which encourages its application for real-time complex water treatment and desalination. Thus, combining the properties of GO and AC and utilizing the composite for water treatment appears rewarding.[36]

The present work reports the preparation and application of AC-GO composites in RO membranes. Optimization of various factors, such as the contact time of MPD and composite loading, followed by an effect on water permeability, salt rejection, and antifouling properties of the prepared TFC membranes, was conducted. The preparation procedures are simple, standard, and feasible, making the overall process scalable and sufficient for brackish water desalination in realistic applications.

2. Result and Discussion

2.1. Characterization of the Starting Materials: Graphene Oxide, Aminoclay, and Aminoclay-Graphene Oxide Composite

Here, we discuss the composite membrane and its characteristics. In view of the detailed studies that are available on them, only essential details are presented, that too in the Experimental Section. Synthesized GO, AC, and AC-GO composites were characterized by UV–vis spectroscopy, Raman spectroscopy, X-ray powder diffraction (XRD), field-emission scanning electron microscopy (FESEM), transmission electron microscopy (TEM), Fourier-transform infrared spectroscopy (FT-IR), and zeta potential measurements (Figures S2–S5, Supporting Information). Figure S2A, Supporting Information shows the UV–vis spectrum of aqueous GO with a characteristic peak at 232 nm and a shoulder at ≈310 nm, which correspond to π–π^* and n–π^* electronic transitions of C=C aromatic bonds and C=O bonds, respectively.[37–39] Figure S2B, Supporting Information represents the Raman spectrum of GO, which showed D- and G-bands at 1339 and 1599 cm^{-1}, respectively. D-band is observed due to structural imperfections created by the attachment of hydroxyl and epoxide groups on GO's carbon basal plane. The G-band is attributed to the metallicity of carbon in graphene, that is, in-plane vibrations.[38,40] The experimental XRD pattern of GO, shown in Figure S2C, Supporting Information, showed a peak at $2\theta = 10°$. It is attributed to the GO lattice's (002) plane, which corresponds to the interlayer spacing of 0.84 nm (expanded greatly from 0.34 nm in graphite).[41,42] TEM images showed a layered structure of nearly-transparent, wrinkled GO sheets (Figure S2D, Supporting Information).

The FESEM images of AC show micron-sized clay sheets (Figure S3A,B, Supporting Information). However, the well-defined layered structure and individual sheets of the clay could not be identified, presumably due to vigorous stirring during their preparation. A schematic of the layered structure of AC and the corresponding TEM image is shown in Figure S4, Supporting Information. Figures S5A,B, Supporting Information display the FESEM images of the AC-GO composite. The EDAX of AC-GO showed the presence of Mg, Si, and Cl, which confirmed the formation of amino-functionalized clay in the composite (Figure S5C, Supporting Information).

XRD patterns recorded for AC and AC-GO composite are shown in **Figure 1**A. AC showed a low angle reflection with a d_{001} interlayer spacing of ≈1.6 nm, which corresponded to the bilayer arrangement of propyl amino groups.[33,43] The broad in-plane reflections at higher angles ($d_{020,110}$ = 0.41 nm, $d_{130,200}$ = 0.238 nm) and the characteristic (060) reflection at $2\theta = 59°$ confirmed the formation of 2:1 tri-octahedral Mg-phyllosilicate clay with a talc-like structure.[33,43] The XRD pattern obtained for the AC-GO composite retained the features obtained for AC and GO individually, with slight shifts in the peak positions, which arose due to the amine's electrostatic interaction with the oxygen-containing groups of GO.[44] Thus, the observed pattern confirmed the formation of the composite with the retention of their chemical integrity. To determine the vibrational features of the AC-GO composite, we performed Raman measurements on AC, GO, and AC-GO composites. Raman spectrum of AC is shown in Figure 1B, which shows multiple peaks. Raman spectrum of GO showed its signature peaks at 1339 (D-band) and 1599 cm^{-1} (G-band). However, we could not observe the spectral feature of aminoclay in the AC-GO composite (Figure 1B), although IR features were observed. A significant Raman feature (both D-and G-band) of GO was observed in AC-GO with a blue shift (≈8 cm^{-1}). The composite exhibited characteristic D- and G-bands of GO at 1331 and 1597 cm^{-1}, respectively. This blue shift is attributed to the hydrogen bonding or electrostatic interaction between the amine of AC with the acid functional group of GO.

FT-IR spectra of GO, AC, and AC-GO composite are shown in Figure 1C. For GO, the broad peak between 3200–3400 cm^{-1} is due to O-H stretching. The peaks at 2975 and 2900 cm^{-1} correspond to asymmetric and symmetric stretching vibrations, respectively, of the CH_2 groups. The IR signals at 1710, 1554, 1410, 1170, and 1045 cm^{-1} are due to C=O stretching, C=C stretching, -OH bending, C-O stretching of epoxy, and C-O stretching vibration of alkoxy functionalities, respectively. For AC, the peaks at ≈3377, ≈2900, ≈2040, 1613, 1126, 1022, and 555 cm^{-1} are due to

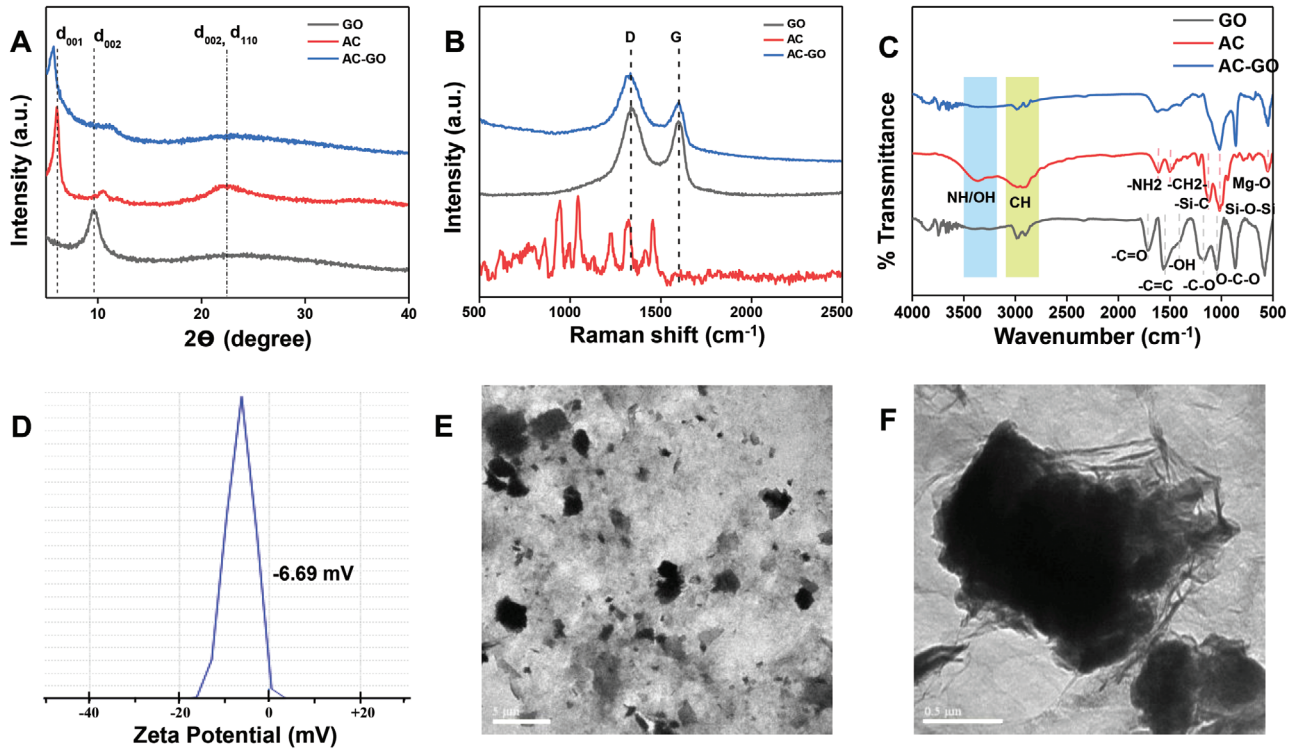

Figure 1. A) XRD pattern, B) Raman spectra, and C) FT-IR Spectra of GO, AC, and AC-GO composite; D) Zeta potential of AC-GO composite; E,F) TEM images of AC-GO composite at different magnifications (scale bars: 5 and 0.5 µm, respectively).

the stretching vibrations of OH, CH_2, NH_3^+, NH_2, Si-C, Si-O-Si, and Mg-O, respectively.[45,46] Also, the signal at ≈1500 cm^{-1} is due to -OH bending. The FT-IR spectrum of the AC-GO composite confirmed the presence of both AC and GO.[39,45,46] Zeta potential measurement of 10:1 (w/w%) AC-GO composite revealed a low negative potential of –6.69 ± 2.95 mV (Figure 1D), which could prove effective in removing water contaminants. This might be due to the presence of oxygen-containing functional groups on the GO sheet in excess of the positively charged moieties on the AC, as the latter has a positive zeta potential.[47] The morphology of the prepared AC-GO composite at different magnifications displayed a stacked lamellar structure having lateral dimensions extending to the micron regime, as explicated from TEM images (Figure 1E,F). Furthermore, the composite showed the presence of clay nanoparticles, viewed as dark features, on the surface of the GO sheet. The negatively-charged GO can form hydrogen bonds or covalent bonds with the terminal primary amine pendant group of the AC, and therefore, might serve as nucleation centers for the clay particles. The negatively charged carbonyl functional groups of GO can also plausibly have electrostatic interactions with the protonated amine moiety.[44] Additionally, Figure S6, Supporting Information showed three types of interactions between AC and GO in AC-GO composites, that is, AC-AC (green shade), GO-GO (red shade), and AC-GO (yellow shade).

2.2. Characterization of Modified TFC Membranes

Desalination takes place by permeation of water molecules diffusing through the membrane, secured in these cells, as presented in **Figure 2**A. Figure 2B further shows the motion of water molecules through the inter-lamellar spacing of the composite. The top surfaces and cross-sections of the AC-GO -modified TFC membranes were characterized using FESEM, and the data were compared with the polysulfone (PSf) substrate and unmodified membranes (TFC), as shown in Figure 2C–E. As shown in Figure 2E, the AC-GO modified (TFC/AC-GO/M30) membranes exhibited unique morphologies and possessed rougher surfaces compared to the PSf support and the other pristine membranes. The TFC/AC-GO membrane showed a typical "ridge and valley" morphology with nodule-like structures, while the PSf and TFC depicted smooth and porous surfaces, respectively. The presence of elements like Mg, Si, and Cl in TFC/AC-GO (Figure 2F) confirmed the coating of AC onto the surface of the membrane.

The FESEM images of the membranes incorporated with varying concentrations of the composite, ranging from 0.005 to 0.100 wt% AC-GO, unveiled diverse morphologies (Figures S7 and S8, Supporting Information). Evidently, the surface morphology of the membranes depends on the percentage of the incorporated composite material. Higher concentrations of AC-GO composite resulted in agglomeration. Similarly, increasing the MPD-substrate contact time resulted in the aggregation of the composite particles (Figure S9, Supporting Information). Excessive loading and extended reaction time are the reasons for such aggregation. Cross-sectional FESEM images revealed the presence of asymmetric, "finger-like" porous structures on the PSf support and the fabric underneath (Figure S10, Supporting Information). However, the polyamide layer was extremely thin and could not be resolved in imaging.

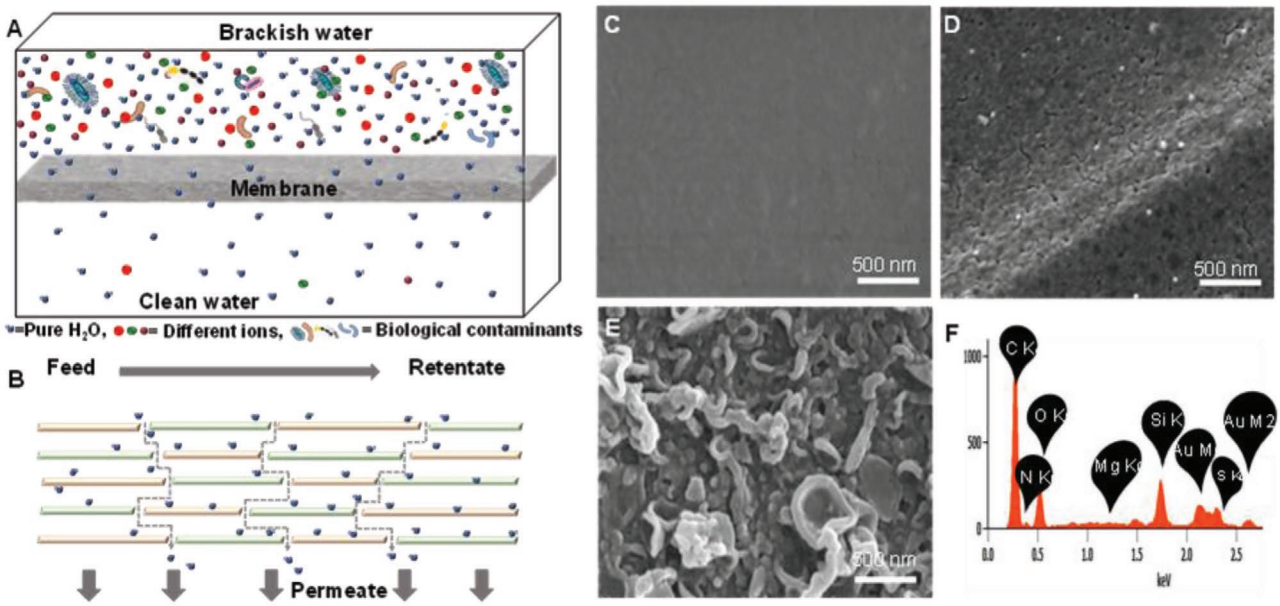

Figure 2. A) Schematic representation of water transport and ions removal across the membrane. B) Detailed mechanism of water transport pathways through the aminoclay-GO sheets. Green and orange bars are representations of aminoclay and GO sheets, respectively. FESEM images of C) Fabric, D) PSf, E) Optimized modified membrane (M30), and F) SEM EDS of the M30 membrane (top view).

Figure S11, Supporting Information shows the FT-IR spectrum of PSf, unmodified TFC, and AC-GO modified membranes. The broad hump centered at 3345 cm^{-1} matched the stretching vibrational frequencies of O-H and N-H groups. Enlarged view of the shaded spectrum showed peaks at 1665, 1583, 1485, 1240, 1150, and 1102 cm^{-1} that correspond to C=O stretching vibration of the amide functional group of the active polyamide layer, N-H, and C-N stretching vibrations of the amide group, C-C stretching, C-O stretching, S=O stretching and =C-H stretching vibrations, respectively, and these are common across all the membranes. However, in membranes other than PSf, two peaks were present at 1546 and 1607 cm^{-1}, which were assigned to N-H bending of the unreacted amine and amide groups, respectively. Conclusively, amide bond formation was observed from the spectra of unmodified TFC and AC-GO modified TFC membranes (M30).

2.3. Permeation Studies of Prepared Membranes

The performance of the prepared membranes was measured in terms of the permeation characteristics like water flux and % of salt rejection efficiency for brackish feed water samples. The data in **Figure 3** represents the outcome of these studies. Figure 3A shows a comparison of the cross-flow permeation results of flux and rejection for the PSf substrate, unmodified TFC (or the PA), and AC (0.015 wt%, TFC/AC), GO (0.015 wt%, TFC/GO), and AC-GO (0.015 wt%, TFC/AC-GO) modified M30 membranes, at 2000 ppm salt and 20 bar pressure. From Figure 3A, it is clear that modified membranes displayed higher water permeation, with improved salt rejection as compared to unmodified PSf membranes. The presence of lamellar nanostructures (TFC/AC and TFC/GO) favored water flow through the membrane matrix. The randomly-positioned nano-sheets (both AC and GO) created channels for water molecules to pass through. Further, the protonated amine moiety of AC and hydrophilic surface functional groups of GO facilitate electrostatic interactions, leading to higher flux than unmodified membranes. The incorporation of AC-GO composite further increased the water flux by 57% (≈1.57×), compared to TFC/AC and TFC/GO, while maintaining a high percentage of salt rejection (>99.5%).

The active layer in modified TFC-RO membranes was the dense polyamide layer, formed by the interfacial polymerization of MPD and TMC. The thickness of this polyamide layer and the amount of material incorporated were a function of contact time between the aqueous diamine solution and the membrane surface. Therefore, to study the effect of contact time of MPD, a set of six membranes, represented as M10 to M60, were prepared by increasing the reaction time of MPD solution with the PSf support (10–60 s), keeping the contact time of TMC solution (50 s) and concentration of AC-GO composite (0.015 wt%) constant.

Figure 3B–D depict an initial increase in water flux from M10 to M30 for all three feed salt concentrations (2000, 5000, and 10 000 ppm), followed by a steady decrease from M30 to M50, and similar for M50 and M60. For feed concentration of 2000 ppm of salt (Figure 3B), M30 exhibited a water flux of 50.28 ± 1.69 L $(m^2\ h)^{-1}$, that is, ≈3.27× higher compared to the unmodified TFC membrane (PA), with 99.51 ± 0.10% salt rejection. For higher salt concentrations of 5000 and 10 000 ppm, water permeation for M30 was 39.23 ± 1.16 and 25.39 ± 0.80 L $(m^2\ h)^{-1}$, with salt rejection efficiencies of 99.41 ± 0.07% and 99.21 ± 0.06%, respectively.

The unprecedented water permeation of the AC-GO modified polyamide matrix membranes was presumably due to the lamellar nanostructures of AC-GO. The stacking of AC on the GO sheets could create transport channels for water

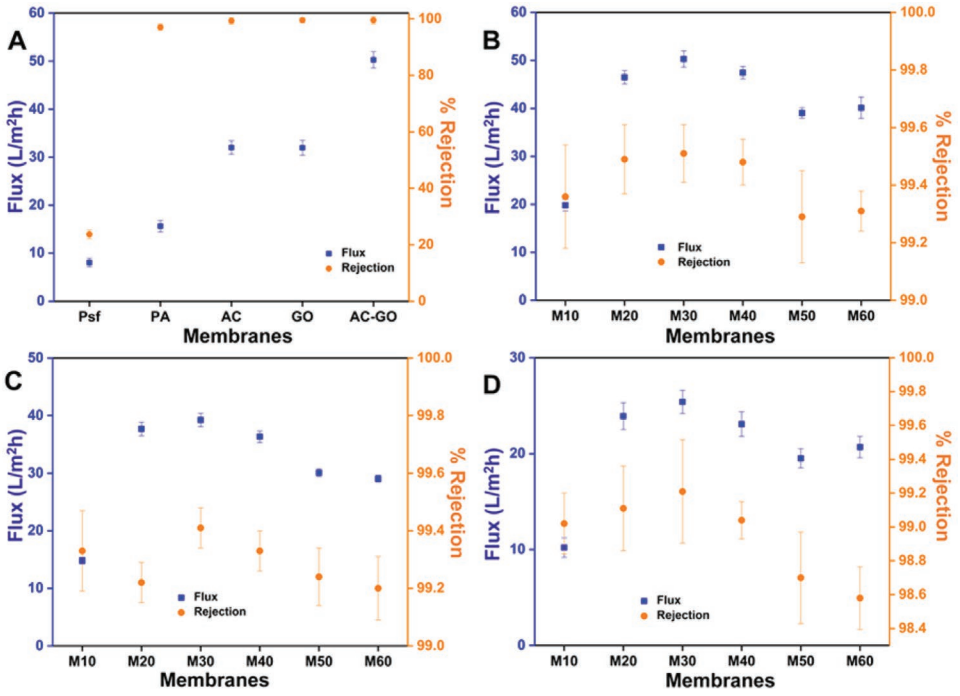

Figure 3. A) Water flux and % salt rejection for PSf support layer, unmodified M30 and modified M30 (0.015 wt% of AC, GO, and AC-GO) at 2000 ppm salt and 20 bar pressure, the average performance of membranes M10-M60 at B) 2000, C) 5000, and D) 10 000 ppm input concentration (feed water), under 20 bar pressure.

molecules and enhance adsorption of water molecules onto the membrane surface and within the inter-lamellar spaces of these stacked structures.[45] In addition, the increase of water permeance might be due to sorption capability in terms of solution-diffusion mechanism due to the presence of hydrophilic functional groups. However, on the contrary, the inclusion of denser nanostructures or higher concentrations of nanomaterials might cause agglomeration of nanosheets, posing resistance to the flow of water molecules, causing a reduction in water flux even at high operating pressures.[48] This agglomeration of 2D materials in the selective membrane layer geometrically leads to reduction in permeance due to the increase in path length. Because of these two opposing effects, an optimum water flux was obtained for TFC/AC-GO (0.015 wt%) M30 among the membranes studied here.

Figure 4A summarizes the study and compares the performance of the membranes at varying input salt concentrations. As observed from Figure 4A, with increasing salt concentration in the feed water sample, the flux declined gradually because of the lower net driving pressure due to the increased osmotic pressure of the feed at higher salt concentration. As the net driving pressure decreased, the relative amount of water passing through the membrane, compared to salt, decreased, resulting in lower salt rejection.

For M30, the water flux observed a continuous increase from 36.12 ± 0.99 to 85.60 ± 1.29 L $(m^2\ h)^{-1}$, corresponding to a pressure variation from 15 to 40 bar (Figure 4B). This direct relationship suggests an increase in the net driving pressure. Higher pressures, in excess of the osmotic pressure, forced the feed water through the membrane, leading to higher permeation and greater flux.[49] Permeation parameters (flux and percentage salt rejection) were plotted as a function of applied pressure to evaluate the membrane's performance. A sharp increase in % salt rejection was observed (98.53 ± 0.17% at 15 bar, to 99.51 ± 0.10% at 20 bar) initially. Further increase in pressure resulted in an insignificant change in % salt rejection, till a pressure of 35 bar. An additional increase of pressure to 40 bar resulted in a slight increase in the % salt rejection (Figure 4B).[50]

Contact angle studies were performed to observe the influence of contact time of the composite and the PSf support on the wettability of the membrane (Figure 4C); and loading of the AC-GO composite on the membranes keeping the contact time constant (Figure 4D). For M10, since the contact time of MPD and the PSf support was too short for nano-composite inclusion into the polymer matrix of the membrane, surface hydrophilicity was only slightly improved when compared to the unmodified membrane (Figure 4C), which was evident from the contact angles for M0 and M10. This slight improvement in surface hydrophilicity was reflected as the rise in flux from 15.62 ± 0.36 to 19.79 ± 1.22 L $(m^2\ h)^{-1}$. When contact time was increased to 50 s, the surface became highly hydrophilic compared to the unmodified membrane. The inclusion of a higher amount of clay composite resulted in the stacking of layers, posing resistance to water flow, thereby decreasing the flux.

Figure 4D shows the effect of incorporating AC-GO composite on the surface hydrophilicity of the thin-film composite membranes, and with an increase in the AC-GO composite concentration from 0 to 0.1 wt% (0–1000 ppm), the variation in water contact angle ($59^{-}55^{0}$), exhibiting improved hydrophilicity.

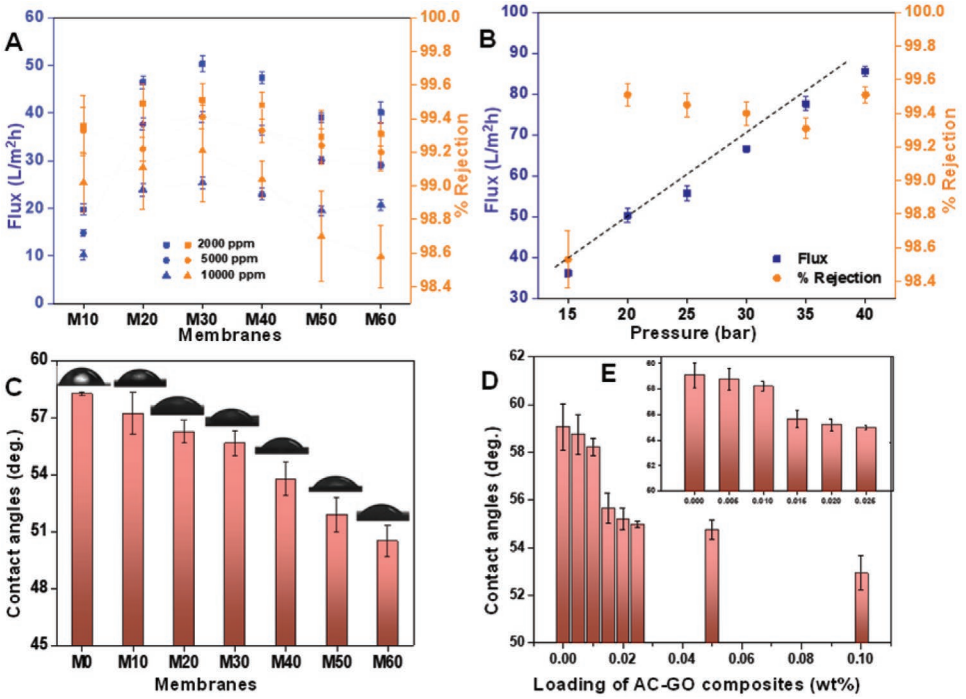

Figure 4. A) Variation in water flux at different feed water concentrations (2000, 5000, and 10 000 ppm), B) Permeation characteristics of M30 with varying pressure at 2000 ppm salt concentration, C) Contact angle of membranes (M0 to M60) with 0.015 wt% AC-GO and D) Contact angle of M30 at different AC-GO loadings and E) expanded view of D. M0 refers to the unmodified TFC.

2.4. Biofouling and Anti-Bacterial Study

To study the resistance of prepared membranes against surface biofouling, model foulant, humic acid was used, and the performance was evaluated in terms of normalized flux, J_n,

$$J_n = J/J_0 \quad (1)$$

where J is the instantaneous flux, and J_0 is the flux after compaction.

A comparative investigation of the antifouling performance of a commercial RO membrane (Vontron: model number: VM-TFC-80), an unmodified M30, and an AC-GO modified M30 was performed by treating them under identical experimental procedures (with 2000 ppm NaCl, 500 ppm humic acid, and 2 mM $CaCl_2$ under 20 bar pressure). **Figure 5**A shows the variation of the normalized flux of membranes with time under testing conditions: 2000 ppm NaCl, 500 ppm humic acid, and 2 mM $CaCl_2$. Before adding foulants to the feed water, compaction was done for 3 h with distilled water to maintain constant flux. During the initial hours of study, a significant reduction in water flux was observed for the commercial membrane, while unmodified and modified M30 showed only a slight decrease in water flux. This indicated that for the commercial membrane, fouling occurred within the first hour of the addition of foulants, perhaps because of high surface roughness and high affinity for humic acid in the feed water. After 3 h of examination, a sharp decline was observed for the unmodified membrane, indicating the deposition of humic acid on its surface. Even after 10 h of the experiment, the AC-GO modified membrane showed only a moderate decrease in water permeation. It implies less bio-fouling of the prepared membrane, plausibly due to the electrostatic repulsions between negatively charged humic acid at brackish water pH and negative zeta potential of the AC-GO composite. This repulsive force was effective in preventing the fouling of membranes incorporated with the clay composite. Since humic acid is hydrophobic, the extent of foulant deposition on the membrane was analyzed by measuring the contact angle on fresh and bio-fouled membranes (Figure 5A).

For the commercial membrane, maximum fouling was observed, and the contact angle changed from 40.7^0 to 60.2^0 in 10 h. For unmodified and modified composite membranes, the angle was observed to increase from 59.1^0 and 55.6^0 to 62.7^0 and 57.4^0, respectively, for the same period (Figure 5B). The difference in the contact angles indicated that scaling had occurred due to the added foulants. For AC-GO modified membrane, the change in angle was found to be the minimum, which suggested improved resistance to such foulants. A larger amount of humic acid was deposited onto the commercial membrane compared to the M30 membrane. The observed result could be attributed to repulsive forces existing between the composite and the foulant.

Figure 5C,D show that the M30 membrane exhibited good bacterial (*Escherichia coli* and *Bacillus subtilis*) growth inhibition, compared to the unmodified and commercial membranes. The M30 membrane showed 90% and 44% anti-bacterial effect on *E. coli* and *B. subtilis*, respectively. This agrees with the known anti-bacterial activity of GO against gram-positive and gram-negative bacteria. The commercial membrane failed to show such anti-bacterial effects, while the M30 membrane showed high stability in resisting bacteria and foulants (Figure 5).

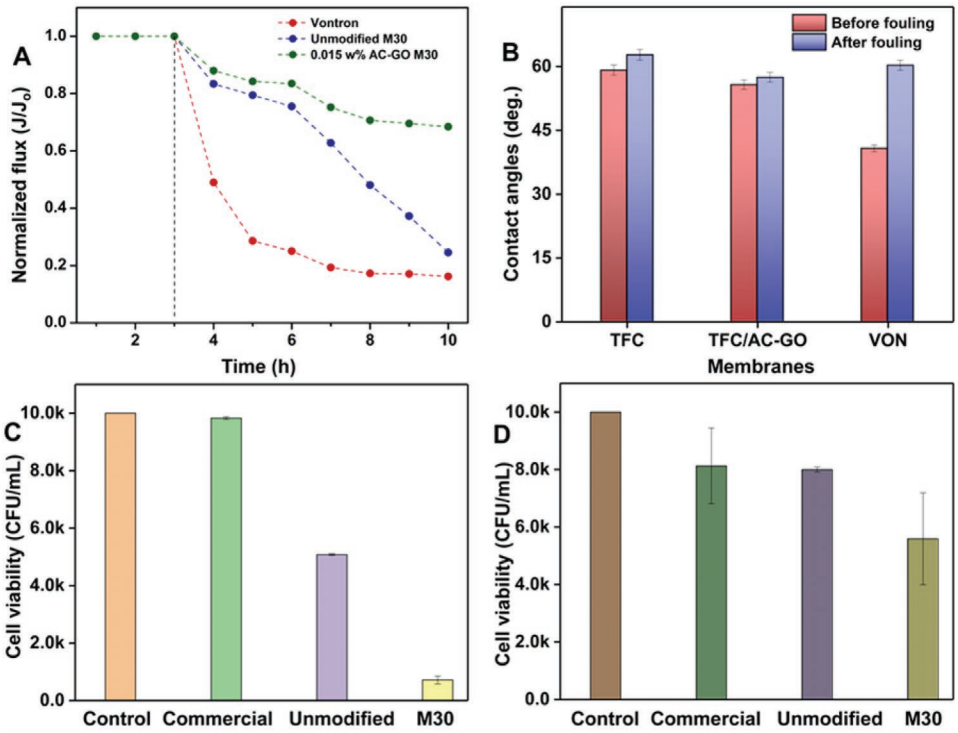

Figure 5. A) Normalized water flux for Von-VM-TFC-80, unmodified M30, and 0.015 wt% AC-GO modified membranes during the antifouling test with 2000 ppm NaCl, 500 ppm humic acid, and 2 mM $CaCl_2$ under 20 bar pressure, B) contact angle for fresh and humic acid-fouled membranes and cell viability test on the membrane with control, commercial, unmodified-TFC and M30 membranes with C) *E. Coli* and D) *B. Subtilis* bacteria after 8 h of incubation.

3. Conclusion

The potential use of TFC-RO membranes, modified with aminoclay-graphene oxide composite, was investigated. The membranes showed improved water flux due to increased surface area and enhanced hydrophilicity, along with enhanced salt rejection. For a feed concentration of 2000 ppm of salt, the membrane M30 modified with 0.015 wt% of composite exhibited a flux of ≈50.28 ± 1.69 L $(m^2\ h)^{-1}$ with 99.51 ± 0.10% salt rejection at 20 bar and 25 °C. The incorporation of AC-GO further increased the water permeation and showed a 57% (≈1.57×) enhancement compared to TFC/AC and TFC/GO membranes while maintaining high salt rejection (>99.5%). Overall, modified M30 membrane flux increased ≈3.27× compared to the unmodified TFC membrane (PA membrane) at 20 bar pressure in 2000 ppm feed NaCl solution. The membranes displayed a reduction in contact angle with an increase in contact time of PSf substrate and MPD, suggesting greater inclusion of composite into the substrate with time. Similar measurements were done for membranes with different composite loadings. The negative zeta potential of the composite was responsible for significantly improving fouling resistance to humic acid. These modified membranes were prepared by employing the standard procedure for interfacial polymerization. Therefore, the approach is simple and scalable to develop membranes for brackish water desalination.

4. Experimental Section

Materials: Natural graphite flakes (95% of carbon) were obtained from Active Carbon. Sulfuric acid (H_2SO_4, 95–98%) and hydrochloric acid (HCl, 36%) were purchased from Rankem Chemicals. Phosphorus pentoxide (P_2O_5, 95%) and hydrogen peroxide (H_2O_2, 98%) were purchased from SD Fine Chemicals. Potassium permanganate ($KMnO_4$, 98.5%) and potassium peroxydisulfate ($K_2S_2O_8$, 98%) were procured from Sisco Research Laboratories. Nitric acid (HNO_3) (65–68%), magnesium chloride ($MgCl_2.6H_2O$), (3-Aminopropyl) triethoxysilane (APTES), and sodium hydroxide (NaOH) were purchased from Merck. Acetone, ethanol, and sodium chloride (NaCl) from Loba Chemie. Polysulfone (PSf, MW 35 000 g mol^{-1}) and trimesoyl chloride (TMC, 99% purity) were procured from Sigma Aldrich. Calcium chloride ($CaCl_2$), oxalic acid, hexane (HPLC grade), dimethylsulfoxide (DMSO), *N*,*N*-dimethylformamide (DMF), and *N*-methyl-2-pyrrolidone (NMP) were purchased from Merck. D(+)– 10-camphor sulfonic acid (CSA) and sodium lauryl sulphate (SLS) were obtained from Spectrochem. m-Phenylenediamine (MPD, 98%) was procured from Alfa Aesar. Sodium lauryl sulfate (SLS), sodium chloride (NaCl), and sodium hypochlorite (NaClO, 6% available free chlorine) were purchased from Rankem. The sodium salt of humic acid (HA) containing 50–60% of HA was procured from Acros Organics. Luria Bertani (LB) Broth and Nutrient agar were purchased from HiMedia. Escherichia coli MTCC 443 and Bacillus subtilis ATCC 21 331 were procured from MTCC and ATCC, respectively. All chemicals were of analytical grade and used as received without further purification. Glassware was cleaned thoroughly with aqua regia (HCl:HNO3, 3:1 vol%), rinsed with deionized water (DI) water, and dried in an oven before use.

Characterization: The UV–vis spectroscopy measurements, in the range 200 to 1100 nm, were performed using PerkinElmer Lambda 25 spectrophotometer. IR spectra of the materials were measured using PerkinElmer Spectrum-One spectrometer, fit with a diamond crystal (for stronger signals due to greater penetration). However, germanium crystal was used for dark samples because of its high-refractive-index. Raman spectra of materials were obtained using WITec GmbH CRM200 confocal Raman spectroscope with 532 and 633 nm laser excitation. Morphological studies of the prepared composite and the membranes, elemental analysis, and elemental mapping were carried out using a

scanning electron microscope equipped with energy dispersive analysis of X-rays (EDAX or EDS) (FEI Quanta 200) and HRTEM (JEOL 3010, 300 kV). Also, HRSEM images of the electrode materials were obtained through Thermo Scientific Verios G4 UC SEM. The experimental XRD patterns were obtained by Bruker D8 Advance X-ray diffractometer with Cu Kα radiation (λ = 1.54 Å). The hydrophilicity of the membranes was obtained by contact angle measurements using a Holmarc contact angle meter.

Preparation of Graphene Oxide: Graphene oxide (GO) was synthesized from graphite powder using a modified Hummer's method.[51,52] Graphite powder was oxidized using concentrated sulphuric acid (H_2SO_4), potassium persulphate ($K_2S_2O_8$), and phosphorus pentoxide (P_2O_5) as oxidizing agents. The resulting dark blue mixture was cooled to room temperature. It was then diluted, filtered with a membrane of 0.22 µm, and dried. The obtained powder was then added to cold H_2SO_4, to which potassium permanganate ($KMnO_4$) was slowly added with continuous stirring in an ice bath. After 15 min, sodium nitrate ($NaNO_3$) was added to the mixture. The solution was further stirred for 2 h at 35 °C and 200 mL distilled water was added slowly to complete the reaction. It was then further diluted with distilled water (≈500 mL), and 15 mL of hydrogen peroxide (H_2O_2) was added for further oxidation. The color of the mixture turned brown-yellow, which indicated the formation of GO. The product was first washed with hydrochloric acid (HCl) (1:10), then with water, and finally suspended in distilled water. The brown dispersion was dialyzed for 7–10 days to remove residual metal ions and acids. GO was then exfoliated via sonication for 1.5 h.

Preparation of Aminoclay: Aminopropyl functionalized aminoclay was prepared by using magnesium chloride ($MgCl_2.6H_2O$) and (3-Aminopropyl) triethoxysilane (APTES) as precursors.[33,53,54] Briefly, 8 g of $MgCl_2.6H_2O$ was added to 150 mL of ethanol in a 250 mL conical flask. To it, 12 mL of APTES was added drop-wise, and the solution was magnetically stirred for 24 h at room temperature to obtain a milky white suspension. The suspension was then aged at 40 °C, followed by centrifugation and washing with ethanol to get the white product, which was then grinded and sieved to produce the powdered material.

Preparation of Aminoclay-Graphene Oxide Composite: Prepared GO and AC were added in 1:10 (w/w%) ratio and left for stirring for 24 h at room temperature to obtain a brown-black slurry. The slurry was dried at 100 °C, followed by redispersion in water, centrifugation, and repeated washing with ethanol. The composite was dried at 60 °C, which was then ground into excellent powder by ball milling for 4 h.

Membrane Casting: The polysulfone (PSf) porous substrate was prepared by the phase inversion process, wherein the non-woven polyester fabric was cast with the polymer-doped solution using a flat RO membrane casting unit. First, the polymer solution (19 wt%) was prepared by dissolving 19 g of polysulfone pellets (Mol. Wt. ≈ 35 kDa) in 78.64 mL of *N*-methyl-2-pyrrolidone (NMP, density: 1.03 g cm^{-3}). The mixture was stirred continuously at 60 °C for 24 h to obtain a homogenous solution, which was subsequently degassed in a desiccator to remove air bubbles. Second, the fabric was placed on a flat glass sheet, and the polymer solution was uniformly spread on it, keeping a thickness of 0.2 mm by an adjustable casting knife. The prepared membranes were placed in DI water and preserved in Milli-Q water at ≈4 °C until further use.[31]

Preparation of Thin-Film Composite (TFC) Membranes: Both unmodified and modified TFC-RO membranes were prepared by interfacial polymerization on a PSf substrate. Detailed experimental conditions for synthesizing GO, AC, and AC-GO composite are provided in the Section 4. Briefly, an aqueous solution containing of m-phenylene diamine (MPD) (2.0 wt%), camphor sulphonic acid (CSA) (1.0 wt%), sodium lauryl sulphate (SLS) (0.2 wt%), and AC-GO composite (0.015 wt% for modified membranes), after probe sonication of 10 min, was allowed to come into contact with the PSf substrate for different time intervals (10, 20, 30, 40, 50, and 60 s, denoted as M10 to M60). The excess solution was drained-off, followed by the reaction with TMC (0.1 wt%) in hexane for 50 s, to induce polymerization between the diamine moiety of MPD and the acid chloride moiety of TMC. The membranes were then cured at 60 °C for 5 min. After thoroughly washing with water, the membranes were stored in Milli-Q water at ≈4 °C until further use.

Performance Studies of Membranes: The modified TFC membranes were analyzed for their performance, based on water flux and salt rejection rates of total dissolved solids (TDS), using a cross-flow permeation apparatus (Figure S1, Supporting Information). Cross-flow refers to the tangential flow of feed water with respect to the membrane. The set-up consisted of three membrane chambers, and each had an effective surface area of 32.3 cm^2. This arrangement allowed the analysis and comparison of the performance of three membranes simultaneously, under identical operating conditions. Unless stated otherwise, the running conditions were 20 bar pressure, room temperature (25 °C), neutral pH, and 3.75 L min^{-1} (225 L h^{-1}) flow rate with a 2000 ppm concentration of NaCl in feed water. However, before adding NaCl to the feed w, the membranes were compacted using distilled water for 3 h to achieve a constant flux. Also, throughout the RO test runs, both permeate and reject water were re-circulated to the feed inlet tank to maintain constant salt concentration during the study. Membrane's resistivity to chloride ions was tested at different NaCl concentrations (2000, 5000, and 10 000 ppm).

The salt rejection (R) and permeation flux (J) for the studies were determined using the following two equations,

$$R = \left(1 - \frac{C_p}{C_f}\right) \times 100\% \tag{2}$$

$$J = \frac{V}{A \cdot t} \tag{3}$$

where C_f and C_p are the salt concentrations in the feed and permeate, respectively, V is the volume of permeate collected over a time interval t for a membrane cross-sectional area, A.

Also, relation between flux (LMH) and permeance (LMH/bar) has been given below,

$$\text{Permeance} = \frac{\text{Flux}}{\text{bar}} \tag{4}$$

where LMH is liter per meter square per hour (L m^{-2} h^{-1}).

Anti-Bacterial Test of Membranes: *E. coli* and *B. subtilis* bacterial stock cultures were revived by inoculation in LB broth and were grown overnight at 37 °C and 120 rpm shaking for 4 h. The culture was used for inoculation into fresh LB broth and allowed to grow till the culture reached the log phase. The bacterial cells were washed twice in saline by centrifugation at 3000 rpm for 5 min to remove the nutrients in the medium. Membranes (commercial, unmodified and modified M30) uniformly cut in the dimensions of 0.5 cm × 0.5 cm were sterilized by spraying 70% ethanol on them and allowed to dry in a laminar flow chamber. These membranes were introduced into 1 mL of 104 CFU mL^{-1} of bacterial cells suspended in saline. The cells were shaken at 80 rpm for 8 h to avoid the settling of bacterial cells and to keep the cells in continuous contact with the membrane. The number of viable cells after incubation with the membranes was determined through the colony counting method by inoculating the cells interacted with the membrane on nutrient agar plates for 24 h at 37 °C. All the experiments were done in triplicates.

Supporting Information

Supporting Information is available from the Wiley Online Library or from the author.

Acknowledgements

MD. R.I., and P.K. contributed equally to this work. The authors thank the Department of Science and Technology (DST) and Nano Mission of India's Government for constantly supporting the research program on nanomaterials. MD.R.I. thanks the Council of Scientific and Industrial

Research (CSIR) for his SRF fellowships. M.J. and M.A.G. thank the University Grants Commission (U. G. C.) for their doctoral fellowship. P.K., P.S., A.N., and S.K.J. thank IIT Madras for their research fellowships.

Conflict of Interest

The authors declare no conflict of interest.

Data Availability Statement

Research data are not shared.

Keywords

aminoclay, desalination, graphene oxide, reverse osmosis, water purification

Received: April 3, 2021
Revised: July 12, 2021
Published online:

[1] V. Albergamo, B. Blankert, E. R. Cornelissen, B. Hofs, W.-J. Knibbe, W. van der Meer, P. de Voogt, *Water Res.* **2019**, *148*, 535.
[2] G. Amy, N. Ghaffour, Z. Li, L. Francis, R. V. Linares, T. Missimer, S. Lattemann, *Desalination* **2017**, *401*, 16.
[3] X. Cheng, W. Zhou, P. Li, Z. Ren, D. Wu, C. Luo, X. Tang, J. Wang, H. Liang, *Chemosphere* **2019**, *234*, 545.
[4] M. Kumar, S. RaoT, A. M. Isloor, G. P. S. Ibrahim, Inamuddin, N. I. , A. F. Ismail, A. M. Asiri, *Int. J. Biol. Macromol.* **2019**, *129*, 715.
[5] A. Tabriz, M. A. Ur Rehman Alvi, M. B. Khan Niazi, M. Batool, M. F. Bhatti, A. L. Khan, A. U. Khan, T. Jamil, N. M. Ahmad, *Carbohydr. Polym.* **2019**, *207*, 17.
[6] X. Wang, H. Ma, B. Chu, B. S. Hsiao, *Desalination* **2017**, *420*, 91.
[7] Z. Yang, Y. Zhou, Z. Feng, X. Rui, T. Zhang, Z. Zhang, *Polymers* **2019**, *11*, 1252.
[8] I. H. Aljundi, *Desalination* **2017**, *420*, 12.
[9] J. E. Cadotte, *Mater. Sci. Synth. Membr.* **1985**, *269*, 273.
[10] M. Elimelech, W. A. Phillip, *Science* **2011**, *333*, 712.
[11] J. E. Cadotte, R. J. Petersen, R. E. Larson, E. E. Erickson, *Desalination* **1980**, *32*, 25.
[12] A. Ismail, M. Padaki, N. Hilal, T. Matsuura, W. J. Lau, *Desalination* **2015**, *356*, 140.
[13] H.-R. Chae, J. Lee, C.-H. Lee, I.-C. Kim, P.-K. Park, *J. Membr. Sci.* **2015**, *483*, 128.
[14] B. Mi, M. Elimelech, *Desalination* **2013**, *312*, 75.
[15] F. Shao, L. Dong, H. Dong, Q. Zhang, M. Zhao, L. Yu, B. Pang, Y. Chen, *J. Membr. Sci.* **2017**, *525*, 9.
[16] D. Manish, P. R. Buch, P. Rao, J. J. Trivedi, A. V. R. Reddy, *IJND* **2008**, *3*, 175.
[17] S. Avlonitis, W. T. Hanbury, T. Hodgkiess, *Desalination* **1992**, *85*, 321.
[18] A. S. Al-Hobaib, K. M. Al-Sheetan, M. R. Shaik, N. M. Al-Andis, M. S. Al-Suhybani, *Nanoscale Res. Lett.* **2015**, *10*, 379.
[19] S. Al Aani, A. Haroutounian, C. J. Wright, N. Hilal, *Desalination* **2018**, *427*, 60.
[20] S. Balta, A. Sotto, P. Luis, L. Benea, B. Van der Bruggen, J. Kim, *J. Membr. Sci.* **2012**, *389*, 155.
[21] M. Elma, C. Yacou, D. Wang, S. Smart, J. Costa, *Water* **2012**, *4*, 629.
[22] K. M. AL-Sheetan, M. R. Shaik, A. S. AL-Hobaib, N. M. Alandis, *J. Nanomater.* **2015**, *2015*, 363175.
[23] H. Huang, X. Qu, H. Dong, L. Zhang, H. Chen, *RSC Adv.* **2013**, *3*, 8203.
[24] M. Kadhom, W. Hu, B. Deng, *Membranes (Basel)* **2017**, *7*, 31.
[25] S. R. Lakhotia, M. Mukhopadhyay, P. Kumari, *Sci. Rep.* **2018**, *8*, 4976.
[26] C. X. C. Lin, L. P. Ding, S. Smart, J. C. D. da Costa, *J. Colloid Interface Sci.* **2012**, *368*, 70.
[27] L. Y. Ng, A. W. Mohammad, C. P. Leo, N. Hilal, *Desalination* **2013**, *308*, 15.
[28] C. Van Goethem, R. Verbeke, M. Pfanmöller, T. Koschine, M. Dickmann, T. Timpel-Lindner, W. Egger, S. Bals, I. F. J. Vankelecom, *J. Membr. Sci.* **2018**, *563*, 938.
[29] G. Xu, J.-N. Wang, C.-J. Li, *Desalination* **2013**, *328*, 83.
[30] Z. Komeily-Nia, L.-T. Qu, J.-L. Li, *Small Sci.* **2021**, *1*, 2000026.
[31] M. Ali, L. Wang, X. Wang, X. Feng, *Desalination* **2016**, *386*, 67;
[32] S. Xia, L. Yao, Y. Zhao, N. Li, Y. Zheng, *Chem. Eng. J.* **2015**, *280*, 720.
[33] K. K. R. Datta, A. Achari, M. Eswaramoorthy, *J. Mater. Chem. A* **2013**, *1*, 6707.
[34] Y.-C. Lee, E. J. Kim, H.-J. Shin, M. Choi, J.-W. Yang, *J. Ind. Eng. Chem.* **2012**, *18*, 871.
[35] Y.-C. Lee, W.-K. Park, J.-W. Yang, *J. Hazard. Mater.* **2011**, *190*, 652.
[36] Y.-C. Lee, E. Jin, S. W. Jung, Y.-M. Kim, K. Chang, J.-W. Yang, S.-W. Kim, Y.-O. Kim, H.-J. Shin, *Sci. Rep.* **2013**, *3*, 1292.
[37] D. C. Marcano, D. V. Kosynkin, J. M. Berlin, A. Sinitskii, Z. Sun, A. Slesarev, L. B. Alemany, W. Lu, J. M. Tour, *ACS Nano* **2010**, *4*, 4806.
[38] L. Peng, Z. Xu, Z. Liu, Y. Wei, H. Sun, Z. Li, X. Zhao, C. Gao, *Nat. Commun.* **2015**, *6*, 5716.
[39] H. Yu, B. Zhang, C. Bulin, R. Li, R. Xing, *Sci. Rep.* **2016**, *6*, 36143.
[40] K. Krishnamoorthy, M. Veerapandian, K. Yun, S.-J. Kim, *Carbon* **2013**, *53*, 38.
[41] K. Garg, R. Shanmugam, P. C. Ramamurthy, *Carbon* **2017**, *122*, 307.
[42] P. Ramesh, S. Bhagyalakshmi, S. Sampath, *J. Colloid Interface Sci.* **2004**, *274*, 95.
[43] K. K. R. Datta, M. Eswaramoorthy, C. N. R. Rao, *J. Mater. Chem.* **2007**, *17*, 613.
[44] A. Achari, K. K. R. Datta, M. De, V. P. Dravid, M. Eswaramoorthy, *Nanoscale* **2013**, *5*, 5316.
[45] Y.-C. Lee, B. Kim, W. Farooq, J. Chung, J.-I. Han, H.-J. Shin, S. H. Jeong, J.-Y. Park, J.-S. Lee, Y.-K. Oh, *Bioresour. Technol.* **2013**, *132*, 440.
[46] V. K. H. Bui, D. Park, Y.-C. Lee, *Chem. Eng. J.* **2018**, *336*, 757.
[47] Y.-X. An, W.-J. Qu, P.-Z. Yu, J.-G. Lü, *Pet. Sci.* **2018**, *15*, 366.
[48] H. Dong, *J. Membr. Sci.* **2015**, *494*, 92.
[49] M. Kadhom, B. Deng, *Microporous Mesoporous Mater.* **2019**, *279*, 82.
[50] W. Zhou, L. Song, *Environ. Sci. Technol.* **2005**, *39*, 3382.
[51] N. I. Zaaba, K. L. Foo, U. Hashim, S. J. Tan, W.-W. Liu, C. H. Voon, *Procedia Eng.* **2017**, *184*, 469.
[52] M. R. Islam, S. S. Gupta, S. K. Jana, P. Srikrishnarka, B. Mondal, S. Chennu, T. Ahuja, A. Chakraborty, T. Pradeep, *Adv. Mater. Interfaces* **2021**, *8*, 2001998.
[53] Y. Fukushima, M. Tani, *J. Chem. Soc., Chem. Commun.* **1995**, *1995*, 241.
[54] R. B. Ferreira, C. R. da Silva, H. O. Pastore, *Langmuir* **2008**, *24*, 14215.

